Material for Mattioli et al. Geology Data Repository

CALIPSO Instrument Locations and Installation Details

After an initial phreatic phase starting in June 1995, andesitic lava erupted to build a dome complex in the summit crater in November 1995, and periodic collapses of parts of the dome produced pyroclastic flows down the various flanks of the volcano from early 1996 onward (Druittt and Kokelaar, 2002). During 2002, the *CALIPSO* (*Caribbean Andesite Lava Island Precision Seismo-geodetic Observatory*) project began installation of instrumentation in four ~200 m boreholes located around the volcano, with additional surface sites completing the array (Mattioli et al., 2004). Each borehole contains a Sacks-Evertson volumetric strainmeter (dilatometer), seismometer and tiltmeter at depth, with a continuous GPS station fixed at the surface (see Fig. 1 in main text (MT)).

Instrument design details and schematics, along with a photo archive of the installation phase of the CALIPSO project may be found at online (http://comp.uark.edu/~mattioli/research/CALIPSO/Intro.html). The closest instrument operating during the July 12 dome collapse at SHV was at AIRS, 5.25 km to the NNW of the volcano (Fig. 1 MT). The instrument was installed at a depth of 180 m below the surface, yielding an elevation of 80 m below mean sea level (bsl). AIRS is situated on the flanks of the Centre Hills, a 1.0-0.5 Ma volcanic complex, and pre-July 12 dilatometer data suggest that earth tides dominate the non-volcanic signal at this station. A second instrument is located at TRNT, 5.91 km NNE of the volcano. This instrument is at a depth of 180 m, corresponding to an elevation of 165 m bsl. It is located 40 m inland from the eastern coastline of Montserrat at Trants Bay. Both sea and earth tides are strongly recorded here. The third instrument is located at GRLD, on a plateau of 2-3Ma volcanic rocks 9.37 km N of the volcano. The instrument is 180 m below the surface, at an elevation of 30 m bsl. Again, earth tides dominate the non-volcanic signal at this station.

Observation Summary Supporting Tsunami Origin for 300 s Dilatometer Signal

We propose that tsunami were generated by dome-collapse pyroclastic flows (PFs) entering the sea at the mouth of the Tar River valley, east of SHV and that the generated waves created an ocean load that was sensed by the CALIPSO dilatometer array. Flotsam strandlines record the cumulative passage of tsunami along the eastern coastline of Montserrat. We reconstruct the collapse history, report unique dilatometer data, which recorded tsunami passage, and present results of hydrodynamic models that yield "predicted" wave characteristics in reasonable agreement with measurements and observations. Tsunami generated by pyroclastic flows entering both lakes and oceans (Young et al., 2002; Locat and Mienert, 2003) have been recorded sparsely, mainly by visual observation of the waves or their resulting 'tide' marks on the shoreline, and only occasionally by tide gauges (Waythomas and Neal, 1998; Ward and Day, 2001; Watts and Waythomas, 2003; Waythomas and Watts, 2003).

We summarize below the observations that support the origin of the 300 s dilatometer signals as a result of PF-generated tsunami waves (all times in UTC):

(1) The strain signals start at ~22:00 UTC on 12 July, synchronous with visual observations of the first pyroclastic flows entering the sea at the TRD.
(2) The amplitude of the strain signals in a packet at any one station is proportional to the intensity of pyroclastic flow generation as deduced from seismic records; our interpretation is that larger volume (also faster, and more energetic) pyroclastic flows excite higher tsunami waves when entering the ocean.
(3) The largest-amplitude package of strain signals occurs at 03:30 UTC on July 13 (peak amplitude from TRNT), ~7 minutes after the largest collapse event around 03:23 13 July (peak amplitude from HARR seismic envelope).
(4) An eruption cloud rising to ~16 km in height was observed by the GOES-12 satellite at 03:45 on 13 July, containing ash rising from pyroclastic flows and material ejected during the first vulcanian explosion.
(5) The tsunami wave arrival at Guadaloupe occurred somewhere between 03:00 and 04:00 13 July (Pelinovsky et al., 2004), which is consistent with the collapse peak

around 03:30 13 July. The travel time required for this wave is approximately 8 minutes {distance/celerity = 50000 m / (9.8 m/s^2 x 1000 m)$^{1/2}$ =~ 500 s}. An abrupt rise of water at the mouth of the Deshaies River occurred at this time consistent with the eruption peak around 03:30 13 July (Pelinovsky et al., 2004; Edmonds and Herd, 2005; Herd et al., 2005).

(6) The relative amplitude of the strain signal at the three dilatometer stations, *i.e.* the unusual strength of the TRNT signal, is consistent with an ocean-loading source given the close proximity of TRNT to the sea and the fact that the TRNT instrument is considerably below sea level.

(7) The strain signals at GRLD and AIRS, while much smaller in amplitude, always seem to lead the signal at TRNT. We infer that this arises because the elastic strain signals are first generated by pyroclastic flow/seawater splash interactions (including explosions) near the TRF source, reaching all three sites by direct paths according to their respective distances from source. The generated tsunami waves then travel alongshore; the signal at TRNT is dominated by the locally passing water wave rather than the much faster initial direct waves.

(8) The phase and timing of the strain signals at AIRS and GRLD suggest a non-point source, which could be interpreted as a moving source.

Tsunami Simulation and Modeling Details

Pyroclastic Flow Models

Momentum and constitutive equations that describe gravity current development and propagation as a function of time are complex in detail (Imran et al., 2001; Iverson and Denlinger, 2001). In contrast, the center of mass motion of dense gravity currents can be approximated by simple equations of motion, whether hot or cold, wet or dry (Pariseau and Voight, 1979; Slingerland and Voight, 1979; Savage and Hutter, 1989). These approximations may be used to describe the motion of basal flow components of pyroclastic currents (Watts and Waythomas, 2003). We implement these ideas into a simple model of gravity current center of mass motion for pyroclastic flows at SHV (Cole et al., 2002), which is similar to that described Watts (1997) and used by Waythomas and Watts (2003) and Watts et al. (2003).

Watts and Waythomas (2003) provide a reasonable differential equation of motion for the instantaneous velocity $u(t)$ along a planar segment, where $\rho_b(t)$ denotes the instantaneous bulk density, ρ_o is the ambient fluid density, C_m is added mass coefficient, g is acceleration of gravity, $C_n(t)$ is instantaneous Coulomb friction coefficient, C_d is total drag coefficient, and $L(t)$ is instantaneous landslide length. The three center of mass motion coefficients $0.9 < C_m \leq 1.8$, $0.05 \leq C_n \leq 0.2$, and $0.7 \leq C_d < 2.1$ have been examined in a sensitivity analysis, varying each over their full estimated ranges, and experiment (Grilli et al., 2002; Brodsky et al., 2003; Enet et al., 2003).

We solve for velocity $u(t)$ of the mass flow over time steps $\Delta t = t - t_i$. We solve for mass position $s(t)$ along the incline by integrating the velocity $u(t)$ numerically over time. Some features of landslide-like deformation can be simply parameterized in terms of the center of mass motion (Watts and Grilli, 2003). These parameters include an acceleration coefficient k_a, a nose coefficient k_n, and a length coefficient k_l. These coefficients show the following ranges: $1 \leq k_a < 2$, $1 \leq k_n < 1.4$, and $0 \leq k_l < 0.8$ (Watts and Grilli, 2003). The debris thickness is found from conservation of mass.

The foregoing model suffices to describe the motion down Tar River valley for the dense underflow component of pyroclastic flows. We use the model to solve for pyroclastic flow impact velocity U_I, impact thickness T_I, duration of underwater motion t_u, and length of underwater runout r_u to construct reasonable tsunami sources.

Previous work in the Cascade Range, Java, and Montserrat (Norris, 1994; Brodscholl et al., 2000; Lavigne et al., 2000; Herd et al., 2006) has demonstrated the capability of seismic networks to quantify pyroclastic flow volumes. At SHV, a qualitative correlation has also been noted between seismic amplitudes and flow volumes (Miller et al., 1998; Calder et al., 2002). A similar approach has been adopted here to reconstruct individual pyroclastic flow volumes (see fig. 4 MT). The HARR surface broadband seismic station recorded effectively the surface waves produced by pyroclastic flows interacting with the

ground; but data from other stations yielded similar results. We integrated the vertical component of the HARR seismic record to obtain a proxy for individual PF volumes (Brodscholl et al., 2000).

We choose to simulate a PF during Part 2 collapse (eruption events 15-19) with nominal volume $V = 7$ x 10^6 m^3. We assume a constant volume per unit width $V/w = 16700$ m^2, a constant bulk density $\rho_b = 1600$ kg/m^3, and an initial length $L(0) = 300$ m for the dense underflow. We constructed a piecewise linear transect along the known pyroclastic flow pathway, roughly headed east and used an initial center of mass position 2150 m from the shoreline, at an elevation of 460 masl.

Event Order	Cluster	Time (DOY:UTC)	Duration minutes	Volume $10x10^6$ m^3	Average Flux m^3/s	Event Discription
1		193:11:00				Small rockfall event, which gradually get larger, and first events that reach the sea
2	Cluster I	193:23:48 - 00:50	122.0	30.9	4221	moderate size pyroclastic flows
3	Cluster II	194:01:50 - 03:00	70.0	50.6	12053	large events; about half the dome collapsed and these events generate the largest waves recorded at TRNT
4	Cluster III	194:03:00 - 04:51	111.0	104.7	15726	
	Cluster III a	194:03:00 - 03:44	44.5	42.9	16083	
	Cluster III b	194:03:45 - 04:19	34.1	36.1	17661	
	Cluster III c	194:04:19 - 04:51	32.4	25.7	13200	less distinct and more complex influence on waves
5	Cluster IV	194:04:51 - 06:37	106.0	23.7	3733	waning moderate events
				210.0		Total volume (Mm^3)

Table 1. Detailed reconstruction of dome collapse events

Using the same initial conditions and transect orientation, we conducted a sensitivity analysis with six random trials covering the full space of the six coefficients identified above. For all six trials, pyroclastic flow impact with the water occurs between $t_I \cong 30-50$ s after eruption, with a mean value of $t_I \cong 41.5$ s. We find mean pyroclastic flow impact velocity $U_I \cong 76$ m/s, duration of underwater motion $t_u \cong 231$ s, and length

of underwater runout $r_u \cong 5225$ m. We assume a typical pyroclastic flow thickness of $T_I \cong 25$ m at impact based on model results. All pyroclastic flows come to rest on the ocean floor at a water depth of around $h \cong 700$ m.

Tsunami Source Characterization
The tsunami profile $\eta(x)$ in the near field may be described approximately by

$$\eta(x) \approx \eta_o \operatorname{sech}^2(x/\lambda_o) \tag{1}$$

where the origin of the x-axis is located in the near field and aligned with flow motion. In Eq. (1), the tsunami amplitude η_0 and tsunami wavelength λ_0 are arbitrary fitting parameters, unlike the highly constrained parameters of solitary waves. The free surface profile perpendicular to the x-axis also follows a *sech*^{2} function, with the shape determined by both conservation of volume and the tsunami wavelength λ_0. In two dimensions, Walder et al. (2003) found that the tsunami amplitude η_0 was well described by the empirical curve fit $\eta_o / h \approx 1.32\left(w\, t_u \sqrt{g\, h^3} \,/\, V \right)^{-0.68}$, where g is the acceleration of gravity; the equation is valid for $2 \le w\, t_u \sqrt{g\, h^3} \,/\, V \le 100$. The tsunami wavelength is given by $\lambda_0 \approx 0.27\, t_u \sqrt{g\, h}$, which has the same functional form for tsunamis generated by submarine landslides (Watts, 1997; Watts et al., 2000; Watts and Waythomas, 2003). We note that the influence of t_u on η_0 has been neglected in many previous discussions of tsunami generation. In addition to the free surface shape described by Eq. (1), a complete initial condition for many water wave equations requires horizontal water velocities underneath the tsunami. Fritz (2002) found experimentally that these water velocities are approximated by solitary wave theory, even if the tsunami itself is strictly not a solitary wave (Synolakis, 1987).

Despite continuity in wave front, different water wave physics are manifested along the front according to the local water depth (Watts, 1997; Watts and Waythomas, 2003). To simulate this, we subdivided the pyroclastic flow entry-arc into subsections, to represent the minimum number required according to wave physics: two subsections in shallow

water on either side of the entry position generate edge waves, two subsections in deeper water generate wave components at some acute angle on either side of the axis of debris flow motion, and one subsection creates wave components along the centerline of debris flow motion, beyond where the material comes to a stop.

In the above model, we have considered a retrogressive collapse of the massive SHV lava dome during the July 2003 events. Other models assume a single sliding mass (Heinrich et al., 1998). In that case, the maximum tsunami wave heights in front (due east) of the impact site (at 3 km) varied from 4 m to 13 m, depending primarily on height of the debris front, and also on speed (Heinrich et al., 1998). These wave height estimates are higher than ours and are a consequence of the significantly larger assumed mass and the complex differences between the initial wave generation models.

Tsunami Propagation

Simulations of wave generation and propagation were completed on a Dell Dimension 2400 Pentium 4 CPU (2.86 GHz) with 1 Gb RAM running Windows XP Professional. Geowave (v1.0) was used for all simulations reported here. The Geowave code properly accounts for wave nonlinearity and handles frequency dispersion in a manner that correctly simulates deep-water waves (Wei et al., 1995; Wei and Kirby, 1995; Chen et al., 2000; Kennedy et al., 2000). Geowave takes the tsunami sources from TOPICS (Grillli and Watts, 1999) and inputs these as initial conditions into FUNWAVE at the characteristic time t_u after debris flow impact, which is different for each of the five tsunami sources. The TOPICS model allows multiple tsunami sources to be constructed for a single tsunami event, if such complexity is needed.

In the current case study, TOPICS requires at least five “debris flow-style” tsunami sources to define the initial conditions for SHV collapse events that are used as input into the water wave propagation model. Watts and Waythomas (2003) adopted a similar approach for a case study of the Aniakchak, Alaska, tsunami of 3500 BP.

Our simulation grid is based on bathymetry and topography in the near shore region around Montserrat, adjusted for the appropriate shoreline configuration of mid-2003. We

constructed a 601 x 701 node grid with 50 m uniform spacing. Typical simulation runs required >48 h of processing time. Using sensitivity analyses, we further demonstrate that submerged landslide volume and runout length are the most important parameters affecting the generation, propagation, and loading of the tsunami as recorded by the strainmeter array (Van Boskirk et al., 2004; Van Boskirk, 2006).

Parameter	Source 1	Source 2	Source 3	Source 4	Source 5
Impact Longitude (UTM)	84200	84250	84025	84000	84050
Impact Latitude (UTM)	48300	47700	47950	48200	47700
CCW Orientation (deg)	10	-170	-80	-65	-95
Final Depth (m)	94	38	680	700	680
Volume (m3)	1125000	1125000	1500000	1500000	1500000
Impact Velocity (m/s)	65	65	76	76	76
Runout Length (m)	400	400	2600	5225	2600
Runout Time (s)	20	30	47	189	47
Width at Shoreline (m)	100	100	100	100	100
Wavelength (m)	164	156	1034	4240	1034
Impact Froude Number	2.1	3.4	0.93	0.92	0.93
Maximum Amplitude (m)	10.4	11.5	0.35	0.021	0.35

Table 2. Summary of TOPICS inputs for PF sources

Ocean Loading and Dilatometer Response

Our modeling is not yet refined enough to draw definitive conclusions about the exact composition of the 300 s strain signal at AIRS and GERS; our preliminary modeling suggests that the onshore impact of the initial wave north of TRV would have produced the largest island-wide signal. The time delay of the strain signals at AIRS and GERS (GERS usually leads AIRS) compared with the co-located seismic signal from pyroclastic flow emplacement is consistent with this inference. The proximity of the TRNT site to the ocean means that local ocean loading dominates any other signal from the tsunami.

The change in mean stress (σ_m) is one-third the sum of the principal stresses, and reworking the elastic solutions for an strip load over half the infinite surface of a half-space (Gray, 1936; Poulos and Davis, 1974) yields the expression, $\sigma_m = (2q\beta/3\pi)(1 + \upsilon)$, where q is vertical distributed load, β is horizontal angle (radians) from the strain sensor to the edge of the distributed load (in this case 0.43π), and υ is Poisson ratio (assumed 0.25). Although this solution assumes infinite loading distributed offshore and parallel to the shore, the stress effect is dominated by the loading closer to the sensor site, and we believe the solution reasonably approximates a long-wavelength water load. The volumetric strain recorded by the *CALIPSO* array therefore represents an areal integration of wave effects over a broad footprint, implying that the dilatometer response likely filters out higher frequency wave forcing. The amplitude of the observed strain signal at TRNT (~0.32 μs when data are bandpass filtered between 0.002 and 0.004 Hz) would require loading by tsunami waves of 0.6 to 1.3 m height (assuming 0.54 μs/m of wave height at 40 m horizontal distance from load edge to instrument or 0.25 μs/m of wave height at 250 m horizontal distance (see MT for discussion). The tsunami simulation shown here yields wave heights between 0.5 and 1.2 m (gauges (f) and (e) below), which itself is consistent with initial tsunami wave heights of ~1.2 m near the source north of TRF (gauge (a) below).

Time series of individual wave gauges from Geowave model simulations are shown in plates **(a)** through **(f)** below. The location of each of the gauges is shown in Fig. 1 (MT) and the individual plates of fig. 4 (MT). The range from TRD to the individual gauge is shown in the upper right corner of each plate. Note the time span for each record is from 0 to 1950 s and the vertical scale is ± 2 m relative to msl. Gauges **(e)** and **(f)** are closest to the TRNT borehole site and the horizontal distance from each gauge to the dilatometer is 392 m and 360 m, respectively. Near the source (TRF, gauge (a)), the wave amplitude is ~1 m for the first several waves, with a trough at -2.5 masl. At White's Bottom (gauge (b) in Fig. 1 and DR) the first wave is highest at ~1.5 m, but at gauges farther north along the coast, the third to fifth waves are larger in amplitude (gauges (c) and (d) in Fig. 1 and DR). Average wave heights were also calculated for a semi-circular array of gauges

arranged in two radial arcs at 250 and 500 m from the TRNT site and these yield maximum wave heights of 0.52 and 0.22 m, respectively.

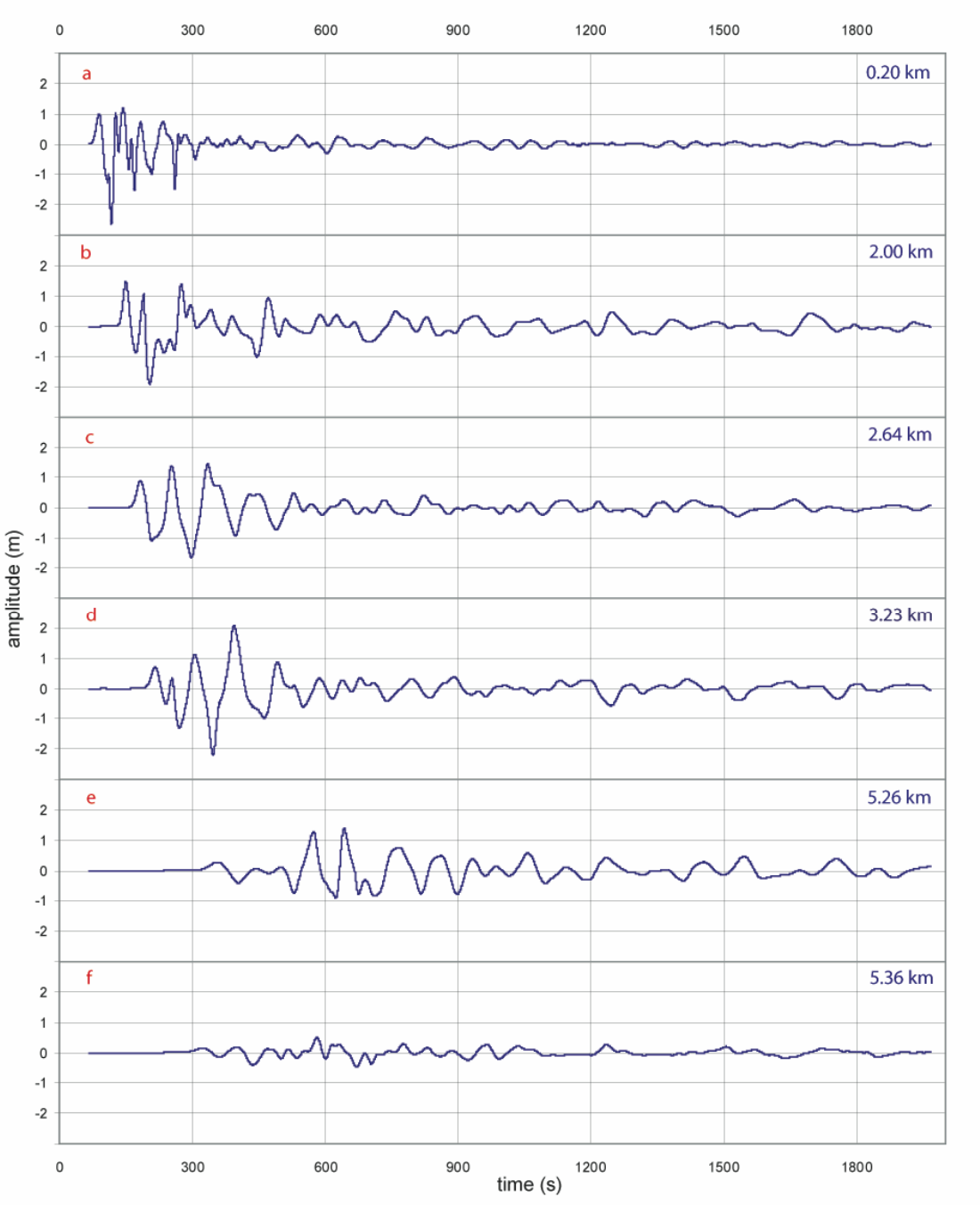

Fig. 1. Numerical wave gauges for tsunami simulation shown in fig. 4 of MT.

References Cited in Data Repository Material

Brodscholl, A., Kirbani, S.B., and Voight, B., 2000, Sequential dome-collapse nuees ardentes analyzed from broadband seismic data, Merapi Volcano, Indonesia: Journal of Volcanology and Geothermal Research, v. 100, p. 363-369.

Brodsky, E.E., Gordeev, E., and Kanamori, H., 2003, Landslide basal friction as measured by seismic waves: Geophysical Research Letters, v. 30, p. 2236-2240.

Calder, E.S., Luckett, R., Sparks, R.S.J., and Voight, B., 2002, Mechanisms of lava dome instability and generation of rockfalls and pyroclastic flows at Soufriere Hills Volcano, Montserrat: Memoir - Geological Society of London, v. 21, p. 173-190.

Chen, Q., Kirby, J.T., Dalrymple, R.A., Kennedy, A.B., and Chawla, A., 2000, Boussinesq modeling of wave transformation, breaking, and inundation. II: 2D: Journal Wtrwy. Port Coast. Oc. Engrg, ASCE, v. 126, p. 48-56.

Cole, P.D., Calder, E.S., Sparks, R.S.J., Clarke, A.B., Druitt, T.H., Young, S.R., Herd, R.A., Harford, C.L., and Norton, G.E., 2002, Deposits from dome-collapse and fountain-collapse pyroclastic flows at Soufriere Hills Volcano, Montserrat: Memoir - Geological Society of London, v. 21, p. 231-262.

Druitt, T.H., and Kokelaar, B.P., 2002, The Eruption of Soufrìere Hills Volcano, Montserrat, from 1995 to 1999, Memoir - Geological Society of London, Volume 21, p. 645.

Edmonds, M., and Herd, R.A., 2005, Inland-directed base surge generated by the explosive interaction of pyroclastic flows and seawater at Soufriere Hills Volcano, Montserrat: Geology, v. 33, p. 245-248.

Enet, F., Grilli, S.T., and Watts, P., 2003, Laboratory experiments for tsunamis generated by underwater landslides, 13th Offshore and Polar Engrg. Conf. : Honolulu, HI, ISOPE03.

Fritz, H.M., 2002, Initial phase of landslide generated impulse waves: Zürich, Switzerland, Eidgenössische Technische Hochschule.

Gray, H., 1936, Stress distribution in elastic solids, Proc. 1st Int. Conf. Soil Mechs. Fndn. Eng., Volume 2, p. 157.

Grilli, S.T., Vogelmann, S., and Watts, P., 2002, Development of a 3D numerical wave tank for modeling tsunami generation by underwater landslides: Engineering Analysis with Boundary Elements, v. 26, p. 301-313.

Grilli, S.T., and Watts, P., 1999, Modeling of waves generated by a moving submerged body. Applications to underwater landslides: Engineering Analysis with Boundary Elements, v. 23, p. 645-656.

Heinrich, P., Mangeney, A., Guibourg, S., Roche, R., Boudon, G., and Cheminee, J.-L., 1998, Simulation of water waves generated by a potential debris avalanche in Montserrat, Lesser Antilles: Geophysical Research Letters, v. 25, p. 3697-3700.

Herd, R.A., Edmonds, M., and Bass, V.A., 2005, Catatrophic lava dome failure at Soufrìere Hills Volcano, Montserrat, 12-13 July 2003: Journal of Vocanology and Geothermal Research, v. in press, p. 19 p.

Imran, J., Parker, G., Locat, J., and Lee, H.J., 2001, 1D numerical model of muddy subaqueous and subaerial debris flows: Journal of Hydraulic Engineering, v. 127, p. 959-968.

Iverson, R.M., and Denlinger, R.P., 2001, Flow of variably fluidized granular masses across three-dimensional terrain; 1, Coulomb mixture theory: Journal of

Geophysical Research, B, Solid Earth and Planets, v. 106, p. 537-552.
Kennedy, A.B., Chen, Q., Kirby, J.T., and Dalrymple, R.A., 2000, Boussinesq modeling of wave transformation, breaking, and inundation. I: 1D: Journal Wtrwy. Port Coast. Oc. Engrg, ASCE, v. 126, p. 39-47.
Lavigne, F., Thouret, J.C., Voight, B., Young, K.D., LaHusen, R.G., Marso, J., Suwa, H., Sumaryono, A., Sayudi, D.S., and Dejean, M., 2000, Instrumental lahar monitoring at Merapi Volcano, central Java, Indonesia: Journal of Volcanology and Geothermal Research, v. 100, p. 457-478.
Locat, J., and Mienert, J., 2003, Evaluating tsunami hazards from debris flows by Walder, J.S. and Watts, P., Submarine Mass Movements and Their Consequences: Dordrecht, Kluwer Academic Publishers, p. 155-162.
Mattioli, G.S., Young, S.R., Voight, B., Steven, R., Sparks, J., Shalev, E., Malin, P., Linde, A., Johnson, W., Hidayat, D., Elsworth, D., Dunkley, P., Herd, R., Neuberg, J., Norton, G., and Widiwijayanti, C., 2004, Prototype PBO instrumentation of CALIPSO Project captures world-record lava dome collapse on Montserrat Volcano: Eos, Transactions, American Geophysical Union, v. 85, p. 317.
Miller, A.D., Stewart, R.C., White, R.A., Luckett, R., Baptie, B.J., Aspinall, W.P., Latchman, J.L., Lynch, L.L., and Voight, B., 1998, Seismicity associated with dome growth and collapse at the Soufriere Hills Volcano, Montserrat: Geophysical Research Letters, v. 25, p. 3401-3404.
Norris, R.D., 1994, Seismicity of rockfalls and avalanches at three Cascade Range volcanoes; implications for seismic detection of hazardous mass movements: Bulletin of the Seismological Society of America, v. 84, p. 1925-1939.
Pariseau, W.G., and Voight, B., 1979, Rockslides and avalanches; basic principles, and perspectives in the realm of civil and mining operations, *in* Voight, B., ed.: Amsterdam, Elsevier Sci. Publ.
Pelinovsky, E., Zahibo, N., Dunkley, P., Edmonds, M., Herd, R., Talipova, T., Kozelkov, A., and Nikolkina, I., 2004, Tsunmai generated by the volcano eruption on July 12-13, 2003 at Montserrat, Lesser Antilles: Science of Tsunami Hazards, v. 22, p. 44-57.
Poulos, H.G., and Davis, E.H., 1974, Elastic solutions for soil and rock mechanics: New York, John Wiley & Sons.
Savage, S.B., and Hutter, K., 1989, The motion of a finite mass of granular material down a rough incline: Journal of Fluid Mechanics, v. 199, p. 177-215.
Slingerland, R.L., and Voight, B., 1979, Occurrences, properties, and predictive models of landslide-generated water waves, *in* Voight, B., ed.: Amsterdam, Elsevier Sci. Publ.
Synolakis, C., 1987, The runup of solaitary waves: Journal of Fluid Mechanics, v. 185, p. 523-545.
Van Boskirk, E.J., 2006, Pyroclastic flow generated tsunami recorded by CALIPSO borehole strainmeters at Soufriere Hills Volcano, Montserrat during massive dome collapse, [M.S. thesis]: Fayetteville, AR, University of Arkansas.
Van Boskirk, E.J., Voight, B., Watts, P., Widiwijayanti, C., Mattioli, G.S., Elsworth, D., Hidayat, D., Linde, A., Malin, P., Neuberg, J., Sacks, S., Shalev, E., Sparks, R.J., and Young, S.R., 2004, Pyroclastic flow generated tsunami waves detected by

CALIPSO borehole strainmeters at Soufriere Hills, Montserrat during massive dome collapse: Numerical simulations and observations: Eos, Transactions, American Geophysical Union, v. 85, p. Fall Meet. Suppl., Abstract OS23B-1315.

Walder, J.S., Watts, P., Soresen, O.E., and Janssen, K., 2003, Tsunamis generated by subaerial mass flows: Journal of Geophysical Research, B, Solid Earth and Planets, v. 108, p. 2236.

Ward, S.N., and Day, S., 2001, Cumbre Vieja Volcano; potential collapse and tsunami at La Palma, Canary Islands: Geophysical Research Letters, v. 28, p. 3397-3400.

Watts, P., 1997, Water waves generated by underwater landslides [Ph.D. thesis]: Pasdena, CA, California Institute of Technology.

Watts, P., and Grilli, S.T., 2003, Underwater landslide shape, motion, deformation, and tsunami generation, Proc. of the 13th Offshore and Polar Engrg. Conf., Volume 3: Honolulu, Hawaii, ISOPE03, p. 364-371.

Watts, P., Grilli, S.T., Kirby, J.T., Fryer, G.J., and Tappin, D.R., 2003, Landslide tsunami case studies using a Boussinesq model and a fully nonlinear tsunami generation model: Natural Hazards and Earth System Sciences, v. 3, p. 391-402.

Watts, P., Imamura, F., and Grilli, S., 2000, Comparing model simulations of three benchmark tsunami generation cases: Science of Tsunami Hazards, v. 18, p. 107-124.

Watts, P., and Waythomas, C.F., 2003, Theoretical analysis of tsunami generation by pyroclastic flows: Journal of Geophysical Research, B, Solid Earth and Planets, v. 108, p. no.12, 21.

Waythomas, C.F., and Neal, C.A., 1998, Tsunami generation by pyroclastic flow during the 3500-year B.P. caldera-forming eruption of Aniakchak Volcano, Alaska: Bulletin of Volcanology, v. 60, p. 110-124.

Waythomas, C.F., and Watts, P., 2003, Numerical simulation of tsunami generation by pyroclastic flow at Aniakchak Volcano, Alaska: Geophysical Research Letters, v. 30, p. no.14, 4.

Wei, G., and Kirby, J.T., 1995, Time-dependent numerical code for extended Boussinesq equations: Journal of Waterway, Port, Coastal and Ocean Engineering, v. 121, p. 251-261.

Wei, G., Kirby, J.T., Grilli, S.T., and Subramanya, R., 1995, A fully nonlinear Boussinesq model for surface waves. I. Highly nonlinear unsteady waves: Journal of Fluid Mechanics, v. 294, p. 71-92.

Young, S.R., Voight, B., Barclay, J., Herd, R.A., Komorowski, J.C., Miller, A.D., Sparks, R.S.J., and Stewart, R.C., 2002, Hazard implications of small-scale edifice instability and sector collapse; a case history from Soufriere Hills Volcano, Montserrat: Memoir - Geological Society of London, v. 21, p. 349-461.